International Symposium
On Turbulence and Shear Flow
Phenomena (TSFP-9)
June 30 - July 3, 2015 *Melbourne, Australia*

PLANE TURBULENT COUETTE FLOW: DNS, LARGE SCALE STRUCTURES AND SYMMETRY INDUCED SCALING LAWS

V. Avsarkisov[1], M. Oberlack[1], S. Hoyas[2], A. Rosteck[1], J. P. Garcia-Galache[2] & A. Frank[1]
[1]Chair of Fluid Dynamics, TU Darmstadt, Otto-Berndt-Str. 2, 64287 Darmstadt, Germany
[2] Motores Térmicos, Univ. Politècnica de València, Camino de Vera S/N, 46022 València, Spain

ABSTRACT

We conducted a set of large scale DNS of turbulent Couette flow with the two key objectives to better understand large scale coherent structures and to validate new Lie symmetry based turbulent scaling laws for the mean velocity and the second order moments.

Direct Numerical Simulation

In this work, a new set of DNSs of a plane turbulent Couette flow has been performed for Reynolds numbers $Re_\tau = 125, 180, 250$ and 550, based on the friction velocity u_τ and on the channel half-width h. Very large computational boxes with variable stream-wise box-length, with $L_x = \lg \cdot 20\pi h$, $L_y = 2h$ and $L_z = 6\pi h$. The flow is periodic in spanwise and streamwise direction. The L_x-parameter $\lg = 2^l$ is given in the subsequent table.

Re_τ	$l=0$	$l=1$	$l=2$	$l=3$
125	x	x	x	x
180	x	x	x	x
250	x	x		x
550	x			

The simulations for the low Re numbers are thus comparable to other, most recent simulations made by Bernardini *et al.* (2013), Tsukahara *et al.* (2006) and the Poiseuille flow at $Re_\tau = 550$ of Jiménez's group (del Álamo & Jiménez, 2003; Jimenez & Hoyas, 2008). A very recent article about this topic is Pirozzoli *et al.* (2014), where the authors analyze a simulation at $Re_\tau = 1000$ in a $18\pi h$ long box.

The code used here was validated in Avsarkisov *et al.* (2014). The numerical scheme is similar to the one used by Kim *et al.* (1987) and Hoyas & Jimenez (2006). The streamwise, wall-normal, spanwise velocity components are u, v and w. The governing equations of the system are transformed into an equation for wall-normal vorticity ω_y and for the Laplacian of the wall-normal velocity $\phi = \nabla^2 v$. The spatial discretization uses dealiased Fourier expansions in x and z, and seven-point compact finite differences in y, with fourth-order consistency and extended spectral-like resolution (Lele, 1992). The wall-normal grid spacing is adjusted to keep the resolution, $\Delta_y = 1.5\eta$, approximately constant in terms of the local isotropic Kolmogorov scale $\eta = (\nu^3/\varepsilon)^{1/4}$ for the $Re_\tau = 550$ case. In wall units, Δy^+ varies from 0.92 at the wall up to $\Delta y^+ \simeq 5.9$ at the centerline. In order to facilitate the comparison of structures in outer variables we used the same grid in wall-normal direction for all $Re_\tau = 180 - 550$ cases. Resolution in x and z is similar to well established simulations of Hoyas & Jimenez (2006), and are approximately $x^+ = 8$ and $z^+ = 4$. The temporal discretization is a third-order semi-implicit Runge-Kutta scheme (Spalart, 1991). Initial fields for the $Re_\tau = 125$ case were taken from previously calculated Poiseuille flows, imposing the new boundary conditions. Initial fields for the rest of the cases were obtained a) increasing the Re_τ or b) interpolating the results of shorter boxes to larger ones.

In order to analyze the inverse of the Kármán constant the log-indicator function $y\partial_y U^+$ has been plotted in figure 1a and 1b for the 180 and 250 cases. All curves collapse well up to their first minimum, at $y^+ \simeq 60$ (not shown). As was suggested

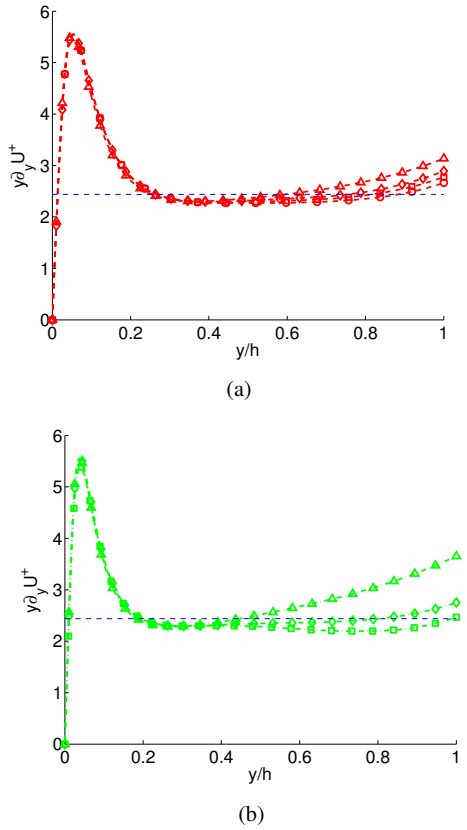

Figure 1: Log-indicator function, (a, b) inverse Kármán constant for (a) $Re_\tau = 180$ and (b) $Re_\tau = 250$ in outer units. The symbols used are: ◊ for $l_x = 20\pi h$, □ for $l_x = 40\pi h$, ○ for $l_x = 80\pi h$ and △ for $l_x = 160\pi h$.

in Hoyas & Jimenez (2006) this value can be taken as a lower limit for the logarithmic layer. The curve in the log-indicator function becomes flatter as we increase the length of the box up to $l_x = 80\pi h$. Since h and U_W are the same for all the simulations, we can employ figure 1 to analyze values of the slope parameter $\Psi = \frac{h}{U_W}\frac{dU}{dy}\Big|_{CL}$. Similarly to the log-indicator function it decreases with increasing box length. However, this changes dramatically for the largest box ($l_x = 160\pi h$) in figure 1. The flatter profile is lost, and the slope parameter increase, almost doubling its value. This may be an indication that the large structures described in the next section greatly affect the flow and that very large boxes are thus needed to describe it.

Large scale coherent structures

From a theoretical point of view the turbulent plane Couette flow is ideal for fundamental investigations on wall-turbulence as it features the convenient property of a constant shear stress across the entire channel height. However, unlike the Poiseuille flow, it is considerably less studied. The main reason for that lies in very large scale structures that are formed in the core region of the plane Couette flow (see e.g. Kitoh &

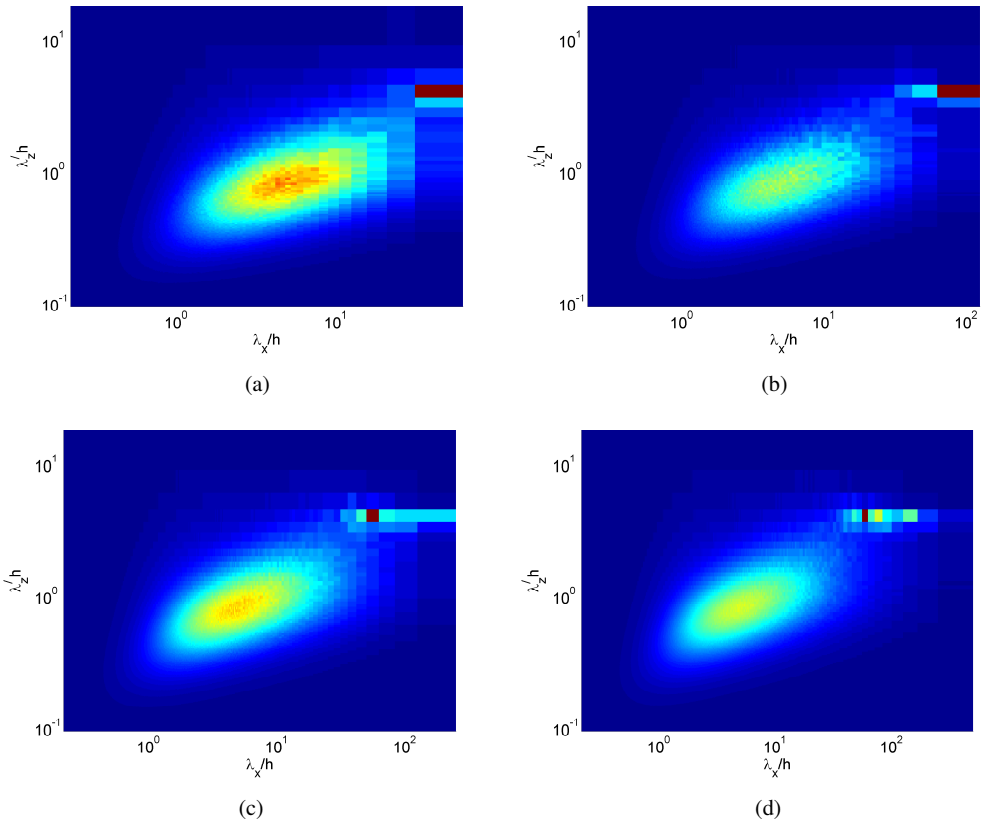

Figure 2: Pre-multiplied spectra at $y^+ \approx 15$ for the $Re_\tau = 125$ case simulated in four different boxes: (a) $l_x = 20\pi h$; (b) $l_x = 40\pi h$; (c) $l_x = 80\pi h$; (d) $l_x = 160\pi h$.

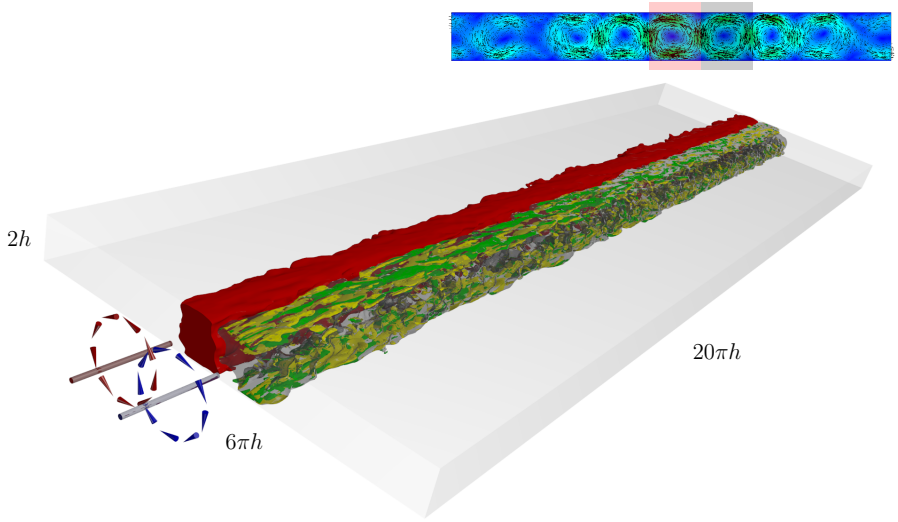

Figure 3: Coherent structures obtained from the ensemble average of the flow field spanning through all the channel and isosurfaces of 10% of the maximum vorticity in spanwise direction at $Re_\tau = 125$.

Umeki, 2008; Tsukahara *et al.*, 2006; Pirozzoli *et al.*, 2011; Bernardini *et al.*, 2013). The necessity of the large numerical boxes to capture these structures makes a numerical study of the plane Couette flow much more computationally expensive than turbulent Poiseuille flow. The footprint of these structures can be appreciated in the pre-multiplied spectra (Hoyas & Jimenez, 2006; Hoyas & Jiménez, 2008). The spectra for the $Re_\tau = 125$ case is plotted in figure 2 for the four boxes. This figure shows the classical spectra at $x^+ = 15$ except for the region at the top-right corner. This part of the spectrum shows that there exist a significant amount of energy on very long and wide scales even in the buffer layer of the flow. Since these structures remain in the flow for a long time their form can be recovered by an ensemble averaging in time, where $x_1 - x_3$

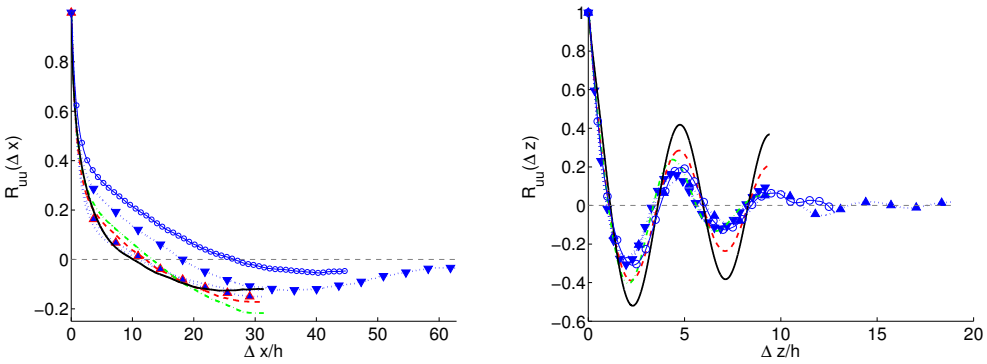

(a) (b)

Figure 4: Two-point autocorrelation coefficient R_{uu} of velocity fluctuations at the centerline, $y/h = 0.5$. (a) Streamwise, (b) Spanwise. Circles from Tsukahara *et al.* (2006). $\triangle$ simulations at $Re_\tau = 125$, $(20\pi h \times 2h \times 12\pi h)$; $\triangledown$, $Re_\tau = 125$, $(40\pi h \times 2h \times 6\pi h)$. The lines are as given in figure 6.

plane averaging has been deactivated. Using such technique we found that the longest structures of the flow appear organized in counter-rotating pairs of rolls with high vorticity at their boundaries. An example of such structures obtained from our DNS at $Re_\tau = 125$ can be taken from figure 3, where we have isolated a pair of counter-rotating rolls. The position of these vortices in the channel is shown in the upper right corner of figure 3. This subplot shows the velocity assembled average of ten turnovers of the simulation. These structures seems to be responsible for the long correlation length observed for Couette flows. The two-point autocorrelation coefficient $R_{uu}(\Delta z)$, is shown in figure 4b. The maxima are all at the same point for all Reynolds numbers studied when $L_z = 6\pi h$. Although it can be seen that the intensity of the autocorrelation $R_{uu}(\Delta z)$ is considerably reduced after $10\Delta z/h$, it still presents a clear sinusoidal pattern, with a distance between extrema of around $1.6\pi h$, i.e., $0.8\pi h$ per structure. This size agrees with those given by other authors, e.g. Tsukahara *et al.* (2006). In the present simulations the autocorrelation coefficient $R_{uu}(\Delta x)$ does not present a secondary extremum below $60h$, as it is shown in figure 4a. An exception is the $Re_\tau = 125$ case, which exhibits an explicit minimum. Thus, in order to capture the longest structures in the higher Reynolds numbers simulations the size of the box must be much larger.

As may be taken from figure 5, the off-wall peak of the streamwise vorticity fluctuation $\omega_x'^+$, which is an indicator for the quasi-streamwise vortices (Jiménez & Pinelli, 1999), is located in the same region as in a pressure-driven channel flow. However, unlike the latter case, here we see the collapse of the vorticity fluctuations profiles from $y^+ = 10$ towards the channel center. It is well known that in the buffer layer, $\omega_y'^+$ has a maximum peak that indicates the existence of velocity streaks. In fact, the location of this peak represents the maximum streak velocity, which is located at $y^+ \sim 15$ in canonical channel flow. The collapse of the wall-normal vorticity fluctuations at different turbulent Reynolds numbers, suggests an invariance of the low-speed streak spacing in wall units (Moser *et al.*, 1999). Similarly to streamwise component, the collapse of spanwise vorticity fluctuation $\omega_z'^+$ profiles occurs beginning with $y^+ = 10$. An almost perfect collapse of all RMS vorticity components in the buffer region of the plane turbulent Couette flow up to $Re_\tau = 550$ implies the presence of the large scale coherent structures in this region which was discussed above. It also suggests that these structures may significantly affect near-wall velocity streaks, quasi-streamwise vortices, ejection and sweep events and consequently the near-wall regeneration cycle.

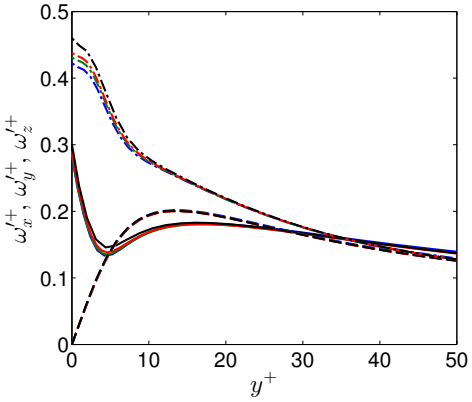

Figure 5: RMS streamwise (—), wall-normal (– –) and spanwise (– · –) vorticity profiles in wall coordinates. Profiles for four Reynolds numbers: $Re_\tau = 125$ (blue), $Re_\tau = 180$ (green), $Re_\tau = 250$ (red) and $Re_\tau = 550$ (black) are taken from Avsarkisov *et al.* (2014).

New symmetries of the correlation equations

Presently, any symmetry we are referring to is a Lie symmetry group which constitutes a transformation that maps equations to itself such as the scaling group $t^* = e^{2a}t$, $x^* = e^a x, T^* = T$ maps the heat equation $T_t = T_{xx}$ to itself i.e. $T^*_{t^*} = T^*_{x^*x^*}$. Apart from deep understanding of the underlaying physics the key properties of Lie symmetries is that they form the basis for constructing invariant solutions, in fluid mechanics often referred to similarity solution if a scaling symmetry is involved. An elementary introduction to the theory of Lie symmetries is given in Hydon (2000).

In order to comprehend the scaling behavior of the mean velocity and higher order correlations of a turbulent Couette we may start with the multi-point correlation equation and its symmetries. Rather different to the classical approach of correlation functions, which is based on the fluctuating values of velocity and pressure, u_i and p, we presently employ the instantaneous

values U_i and P for the correlation. For this we define

$$H_{i_{\{n+1\}}} = H_{i_{(0)}i_{(1)}\ldots i_{(n)}} = \overline{U_{i_{(0)}}(\boldsymbol{x}_{(0)},t)\cdot\ldots\cdot U_{i_{(n)}}(\boldsymbol{x}_{(n)},t)} \ , \quad (1)$$

where the index i of the farthermost left quantity refers to its tensor character, while its superscript in curly brackets denotes the tensor order. The mean velocity is given by the first order tensor as $H_{i_{\{1\}}} = H_{i_{(0)}} = \bar{U}_i$. Using (1) and employing the Navier-Stokes equation we derive the multi-point correlation equation

$$\mathscr{S}_{i_{\{n+1\}}} = \frac{\partial H_{i_{\{n+1\}}}}{\partial t} + \sum_{l=0}^{n}\left[\frac{\partial H_{i_{\{n+2\}}[i_{(n+1)}\mapsto k_{(l)}]}[\boldsymbol{x}_{(n+1)}\mapsto \boldsymbol{x}_{(l)}]}{\partial x_{k_{(l)}}} + \frac{\partial I_{i_{\{n\}}[l]}}{\partial x_{i_{(l)}}} - \nu\frac{\partial^2 H_{i_{\{n+1\}}}}{\partial x_{k_{(l)}}\partial x_{k_{(l)}}}\right] = 0 \text{ for } n = 1,\ldots,\infty \ . \quad (2)$$

where we need to further define

$$H_{i_{\{n+2\}}[i_{(n+1)}\mapsto k_{(l)}]}[\boldsymbol{x}_{(n+1)}\mapsto \boldsymbol{x}_{(l)}] = \overline{U_{i_{(0)}}(\boldsymbol{x}_{(0)},t)\cdot\ldots\cdot U_{i_{(n)}}(\boldsymbol{x}_{(n)},t)U_{k_{(l)}}(\boldsymbol{x}_{(l)},t)} \ , \quad (3)$$

and

$$I_{i_{\{n\}}[l]} = \overline{U_{i_{(0)}}(\boldsymbol{x}_{(0)},t)\cdot\ldots\cdot P(\boldsymbol{x}_{(l)},t)\cdot\ldots\cdot U_{i_{(n)}}(\boldsymbol{x}_{(n)},t)}. \quad (4)$$

Equation (2) may finally completed by continuity equations for all correlations (Rosteck, 2014) which are not shown here.

Investigating this system with respect to its symmetries we naturally observe that it admits all symmetries of Navier-Stokes equations, i.e. the Galilean group plus some scaling symmetries (see e.g. Rosteck, 2014). Here we will only give the two scaling groups needed below, which in the limit of vanishing viscosity read

$$T_{s1}: t^* = t,\ \boldsymbol{x}^* = e^{a_1}\boldsymbol{x},\ \boldsymbol{r}_{(j)*} = e^{a_1}\boldsymbol{r}_{(j)},\quad H^*_{i_{\{n\}}} = e^{na_1}H_{i_{\{n\}}}, I^*_{i_{\{n\}}} = e^{(n+2)a_1}I_{i_{\{n\}}}, \quad (5)$$

referring to scaling of space, while scaling of time reads

$$T_{s2}: t^* = e^{a_2}t,\ \boldsymbol{x}^* = \boldsymbol{x},\ \boldsymbol{r}_{(j)*} = \boldsymbol{r}_{(j)},\quad H^*_{i_{\{n\}}} = e^{-na_2}H_{i_{\{n\}}}, I^*_{i_{\{n\}}} = e^{-(n+2)a_2}I_{i_{\{n\}}}. \quad (6)$$

Most important, however, the system (1) admits additional symmetries, of purely statistical nature. They were first recognized in Oberlack & Rosteck (2010) and significantly extended in Rosteck (2014).

These symmetries for the **H**-**I**-system (2) can be separated into three distinct and generic sets of symmetries

$$\bar{T}_1': t^* = t,\ \boldsymbol{x}^* = \boldsymbol{x},\ \boldsymbol{r}^*_{(l)} = \boldsymbol{r}_{(l)} + \boldsymbol{a}_{(l)},\quad \mathbf{H}^*_{\{n\}} = \mathbf{H}_{\{n\}},\ \mathbf{I}^*_{\{n\}} = \mathbf{I}_{\{n\}}, \quad (7)$$

$$\bar{T}'_{2_{\{n\}}}: t^* = t,\ \boldsymbol{x}^* = \boldsymbol{x},\ \boldsymbol{r}^*_{(l)} = \boldsymbol{r}_{(l)},\quad \mathbf{H}^*_{\{n\}} = \mathbf{H}_{\{n\}} + \mathbf{C}_{\{n\}},\ \mathbf{I}^*_{\{n\}} = \mathbf{I}_{\{n\}} + \mathbf{D}_{\{n\}}, \quad (8)$$

$$\bar{T}_s': t^* = t,\ \boldsymbol{x}^* = \boldsymbol{x},\ \boldsymbol{r}^*_{(l)} = \boldsymbol{r}_{(l)},\quad \mathbf{H}^*_{\{n\}} = \mathrm{e}^{k_s}\mathbf{H}_{\{n\}},\ \mathbf{I}^*_{\{n\}} = \mathrm{e}^{k_s}\mathbf{I}_{\{n\}}. \quad (9)$$

all of which are of purely statistical nature. In the specific case of turbulent parallel shear flows, where x_2 is the wall-normal coordinate, an additional set of symmetries is admitted (see Rosteck, 2014) given by

$$\bar{T}'_{z_{\{n\}}}: t^* = t,\ x_2^* = x_2,\ \boldsymbol{r}^*_{(l)} = \boldsymbol{r}_{(l)},\quad \mathbf{H}^*_{\{n\}} = \mathbf{H}_{\{n\}} + \mathbf{A}_{\{n\}}x_2,\ \mathbf{I}^*_{\{n\}} = \mathbf{I}_{\{n\}}. \quad (10)$$

For the derivation of the symmetries (7), (8), (9) it was crucial to use the form (2) while in the following we concentrate on two-point correlations and Reynolds stresses which are based on fluctuations u_i and p.

In order to use the aforementioned symmetries for constructing invariant solutions and, finally, compare it to correlations such as the Reynolds stress tensor, we may employ Reynolds decomposition $U_i = \bar{U}_i + u_i$ and $P = \bar{P} + p$ to derive relations between the classical and above definitions of correlations

$$H_{i_{(0)}} = \bar{U}_{i_{(0)}} \ , \quad (11)$$

$$H_{i_{(0)}i_{(1)}} = \bar{U}_{i_{(0)}}\bar{U}_{i_{(1)}} + R_{i_{(0)}i_{(1)}} \ , \quad (12)$$

$$H_{i_{(0)}i_{(1)}i_{(2)}} = \bar{U}_{i_{(0)}}\bar{U}_{i_{(1)}}\bar{U}_{i_{(2)}} + R_{i_{(0)}i_{(1)}}\bar{U}_{i_{(2)}} + R_{i_{(0)}i_{(2)}}\bar{U}_{i_{(1)}} + R_{i_{(1)}i_{(2)}}\bar{U}_{i_{(0)}} + R_{i_{(0)}i_{(1)}i_{(2)}} \quad (13)$$

where the Reynolds stress tensor $\overline{u_iu_j}(\boldsymbol{x})$ and the two-point correlation tensor $R_{ij}(\boldsymbol{x},\boldsymbol{r}) = \overline{u_i(\boldsymbol{x})u_j(\boldsymbol{x}+\boldsymbol{r})}$ are connected by the relation $\overline{u_iu_j}(\boldsymbol{x}) = \lim_{\boldsymbol{r}\to 0}R_{ij}(\boldsymbol{x},\boldsymbol{r})$ and $\bar{U}_i$ is the mean velocity. With this the Reynolds averaged Navier-Stokes equation

$$\frac{\bar{\mathrm{D}}\bar{U}_i}{\bar{\mathrm{D}}t} = -\frac{\partial\bar{P}}{\partial x_i} + \nu\frac{\partial^2\bar{U}_i}{\partial x_k\partial x_k} - \frac{\partial\overline{u_iu_k}}{\partial x_k},\ i = 1,2,3, \quad (14)$$

and the two-point correlation equation read

$$\frac{\bar{\mathrm{D}}R_{ij}}{\bar{\mathrm{D}}t} + R_{kj}\frac{\partial\bar{U}_i(\boldsymbol{x},t)}{\partial x_k} + R_{ik}\left.\frac{\partial\bar{U}_j(\boldsymbol{x},t)}{\partial x_k}\right|_{\boldsymbol{x}+\boldsymbol{r}} + \left[\bar{U}_k(\boldsymbol{x}+\boldsymbol{r},t) - \bar{U}_k(\boldsymbol{x},t)\right]\frac{\partial R_{ij}}{\partial r_k} + \frac{\partial\overline{pu}_j}{\partial x_i} - \frac{\partial\overline{pu}_j}{\partial r_i} + \frac{\partial\overline{u_ip}}{\partial r_j} - \nu\left[\frac{\partial^2R_{ij}}{\partial x_k\partial x_k} - 2\frac{\partial^2R_{ij}}{\partial x_k\partial r_k} + 2\frac{\partial^2R_{ij}}{\partial r_k\partial r_k}\right] + \frac{\partial R_{(ik)j}}{\partial x_k} - \frac{\partial}{\partial r_k}\left[R_{(ik)j} - R_{i(jk)}\right] = 0 \ . \quad (15)$$

Using (11)-(13), the statistical symmetries (7)-(10) may be rewritten for the one-point quantities $\bar{U}_i$ and $\overline{u_iu_j}$. From (9) we find

$$\bar{T}_s': \ t^* = t,\ \ \boldsymbol{x}^* = \boldsymbol{x},\ \ \bar{U}_i^* = \mathrm{e}^{a_s}\bar{U}_i,\quad \overline{u_iu_j}^* = \mathrm{e}^{a_s}\left[\overline{u_iu_j} + (1-\mathrm{e}^{a_s})\bar{U}_i\bar{U}_j\right],\ \cdots. \quad (16)$$

where the first two of an infinite row of symmetries (8) are given by

$$\bar{T}'_{2_{\{1\}}}: \ t^* = t,\ \ \boldsymbol{x}^* = \boldsymbol{x},\ \ \bar{U}_i^* = \bar{U}_i + C_i,\quad \overline{u_iu_j}^* = \overline{u_iu_j} + \bar{U}_i\bar{U}_j - (\bar{U}_i + C_i)\left(\bar{U}_j + C_j\right),\ \cdots \quad (17)$$

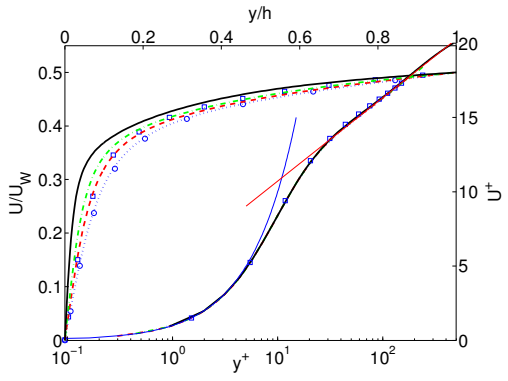

(a)

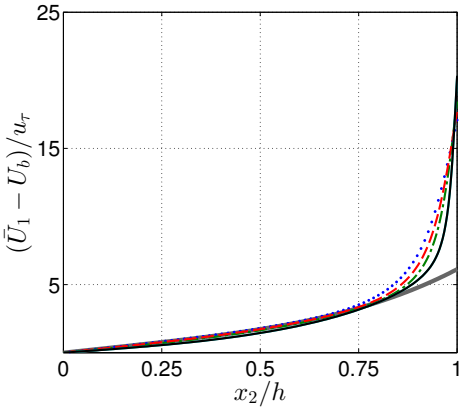

(b)

Figure 6: (*a*) Mean velocity profile scaled in outer (top-left, U_W, h) and inner (bottom-right, u_τ, y^+) scales. Circles from Tsukahara *et al.* (2006); squares from Bernardini *et al.* (2013). Blue solid line corresponds to viscous sublayer linear scaling law; red solid line represents near-wall classical log-law. (*b*) Mean velocity profiles in velocity deficit form normalized on u_τ. ——, profile (23). The simulations at $Re_\tau = 125$ ·····; $Re_\tau = 180$ – – – –; $Re_\tau = 250$ —·— and $Re_\tau = 550$ —— are taken from Avsarkisov *et al.* (2014).

and

$$\bar{T}'_{2_{\{2\}}}: \; t^* = t, \;\; \boldsymbol{x}^* = \boldsymbol{x}, \;\; \bar{U}_i^* = \bar{U}_i, \\ \overline{u_i u_j}^* = \overline{u_i u_j} + C_{ij}, \;\; \cdots . \tag{18}$$

where in the above groups a_s, C_i and C_{ij} are group parameter.

Finally, (10) may reformulated accordingly such that for the mean velocity it has the form

$$\bar{T}'_{z_{\{1\}}}: \;\; x_2^* = x_2, \;\; \bar{U}_1^* = \bar{U}_1 + b_1 x_2, \;\; \overline{u_i u_j}^* = \overline{u_i u_j}, \;\; \cdots \tag{19}$$

while for the stresses we similarly obtain

$$\bar{T}'_{z_{\{2\}}}: \;\; x_2^* = x_2, \;\; \bar{U}_1^* = \bar{U}_1, \;\; \overline{u_i u_j}^* = \overline{u_i u_j} + b_{ij} x_2, \;\; \cdots . \tag{20}$$

Though Rosteck (2014) showed that (10), or more precisely (20), plays an important role for the second moments scaling laws for various shear flow, including the present one as it may be also taken from figure 7, so far data never substantiated (19) for the mean velocity of any wall-bounded shear.

However, with the present large scale DNS of the turbulent Couette flow (19) can clearly be validated and is part of a new Couette flow scaling law to be shown in (23).

Group invariant solutions

From the set of all symmetries given above me may now construct invariant solutions which may be interpreted as turbulent scaling laws. The group invariant solutions may only be properly constructed from the infinitesimal form of the groups (16)-(20) (see e.g. Hydon, 2000). For this it is important to note that infinitesimals form a linear vector space and hence may be combined linearly. Without giving details of its derivation we present the invariant surface condition

$$\frac{\mathrm{d}x_2}{a_1 x_2 + a_4} = \frac{\mathrm{d}\bar{U}_1}{(a_1 - a_2 + a_s)\bar{U}_1 + C_1 + b_1 x_2} = \frac{\mathrm{d}R_{11}}{\xi_{R_{11}}} \ldots \tag{21}$$

where its integration defines the invariant solutions for the moments. Interesting enough, for the present case of a turbulent Couette flow all symmetries appear to be active, i.e. all group parameter in (21) are non-zero and lead to the group invariant solution (23) for the mean velocity. Accordingly, this leads to the second moments (24)/(25), while details are skipped.

Turbulent scaling laws

The mean velocity profiles are shown in figure 6a scaled in outer and inner units. The new profiles agree well with the simulations of Tsukahara *et al.* (2006) and Bernardini *et al.* (2013) at $Re_\tau = 125 - 250$. In figure 6a the log law $U^+ = 1/\kappa \log(y^+) + B$ has been plotted for $\kappa = 0.41$ and $B = 5.1$. Unlike the results of Kitoh *et al.* (2005) and Tsukahara *et al.* (2006) we do not see any dependency of B on the friction Reynolds number in the range $Re_\tau = 125 - 550$. This may be an indication that the Reynolds numbers used in the past were not not sufficiently high to investigate the near-wall log-law. Based on the present DNS data, the classical deficit law known for boundary layer, plane and round Poiseuille flow has been extended to plane Couette flow:

$$\frac{\bar{U}_1 - U_B}{u_\tau} = f\left(\frac{x_2}{h}\right), \tag{22}$$

where the bulk velocity is defined as $U_B = \frac{1}{2h}\int_0^{2h} \bar{U}_1(x_2) dx_2 = \frac{U_W}{2}$ and U_W is the moving wall velocity. A nice validation comprising all our present DNS is given in figure 6b. The classical Couette scaling is in clear contrast to (22), as it is based on a normalization using U_W instead of u_τ. The determination of f in (22) is done using the new symmetries above together with the invariance condition (21).

The new symmetry (19) plays an important role for the Couette flow as it has never been identified in any other turbulent shear flow in Rosteck (2014), while for the Couette flow we find $b_1 \neq 0$. Omitting any details, the final formula for the new scaling of the Couette flow has the following form

$$\frac{\bar{U}_1 - U_b}{u_\tau} = a\frac{x_2}{h} + b\left(\frac{x_2}{h}\right)^n . \tag{23}$$

The latter is shown as solid line in figure 6b, where the values have been determined to $a = 3.046$, $b = 3.081$ and $n = 3.922$. It should be noted that it is in fact the linear part in (23) that

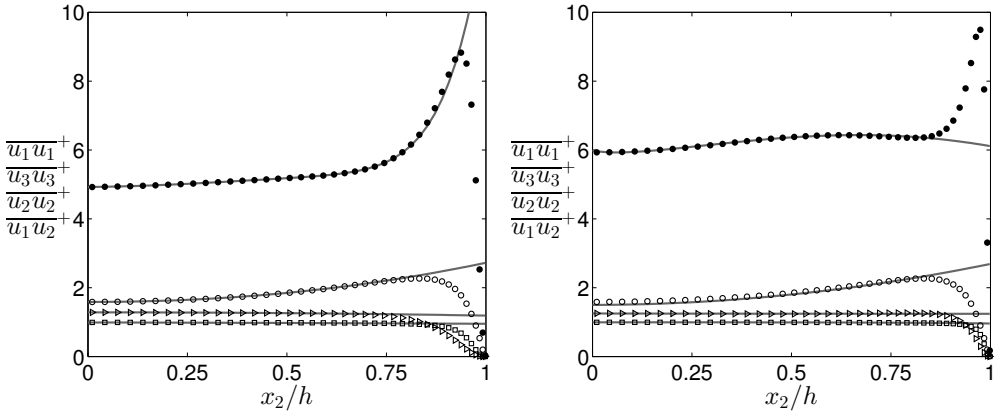

Figure 7: Turbulent shear stresses at (*a*) $Re_\tau = 250$; (*b*) $Re_\tau = 550$. •, $\overline{u_1u_1}^+$; ∘, $\overline{u_3u_3}^+$; △, $\overline{u_2u_2}^+$; □, $\overline{u_1u_2}^+$. Solid lines correspond to the symmetry based theory.

corresponds to the above mentioned new symmetry (19) and, most important, a very precise match of the data is impossible without having this term non-zero.

The corresponding stresses read

$$\frac{R_{ij} - R_{ij}^{cl}}{u_\tau^2} = C_{ij}\left(\frac{x_2}{h}\right)^m \quad \text{for} \quad ij = 12, 22, 33 \qquad (24)$$

and

$$\frac{R_{11} - R_{11}^{cl}}{u_\tau^2} = b_1\left(\frac{x_2}{h}\right)^{2n} + b_2\left(\frac{x_2}{h}\right)^{n+1} + b_3\left(\frac{x_2}{h}\right)^n + b_4\left(\frac{x_2}{h}\right)^2 + b_5\left(\frac{x_2}{h}\right) + C_{11}\left(\frac{x_2}{h}\right)^m, \qquad (25)$$

where R_{ij}^{cl} are the centerline values and, for a given flow, values for n and m are the same in (23)-(25).

REFERENCES

del Álamo, J. C. & Jiménez, J. 2003 Spectra of the very large anisotropic scales in turbulent channels. *Physics of Fluids* **15** (6), L41–L44.

Avsarkisov, V., Hoyas, S., Oberlack, M. & Garcia-Galache, J.-P. 2014 Turbulent plane couette flow at moderately high reynolds number. *J. Fluid Mech R1* **751**, R1–1–10.

Bernardini, M., Pirozzoli, S. & Orlandi, P. 2013 The effect of large-scale turbulent structures on particle dispersion in wall-bounded flows. *International Journal of Multiphase Flow* **51**, 55–64.

Hoyas, S. & Jimenez, J. 2006 Scaling of the velocity fluctuations in turbulent channels up to $re_\tau = 2003$. *Physics of Fluids* **18** (1), 011702.

Hoyas, S. & Jiménez, J. 2008 Reynolds number effects on the reynolds-stress budgets in turbulent channels. *Physics of Fluids* **20** (10), 101511.

Hydon, P.E. 2000 *Symmetry Methods for Dierential Equations. A Beginner's Guide.*. Cambridge University Press, UK.

Jimenez, J. & Hoyas, S. 2008 Turbulent fluctuations above the buffer layer of wall-bounded flows. *J, Fluid Mech.* **611**, 215–236.

Jiménez, J. & Pinelli, A. 1999 The autonomous cycle of near-wall turbulence. *J. Fluid Mech.* **389**, 335–359.

Kim, J, Moin, P. & R, Moser. 1987 Turbulence statistics in fully developed channels flows at low reynolds numbers. *J. Fluid Mech* **320**, 259–285.

Kitoh, O., Nakabyashi, K. & Nishimura, F. 2005 Experimental study on mean velocity and turbulence characteristics of plane couette flow: Low-reynolds-number effects and large longitudinal vortical structure. *J, Fluid Mech.* **539**, 199–227.

Kitoh, O. & Umeki, M. 2008 Experimental study on large-scale streak structure in the core region of turbulent plane couette flow. *Physics of Fluids* **20** (2), 025107.

Lele, S. K. 1992 Compact finite difference schemes with spectral-like resolution. *Journal of Computational Physics* **103** (1), 16–42.

Moser, R. D., Kim, J. & Mansour, N. N. 1999 Direct numerical simulation of turbulent channel flow up to $re_\tau = 590$. *Phys. Fluids* **11** (4), 943–945.

Oberlack, M. & Rosteck, A. 2010 New statistical symmetries of the multi-point equations and its importance for turbulent scaling laws. *Discrete Contin. Dyn. Sys., Ser. S* **3**, 451–471.

Pirozzoli, S., Bernardini, M. & Orlandi, P. 2011 Large-scale motions and inner/outer layer interactions in turbulent couet-tepoiseuille flows. *J. Fluid Mech* **680**, 534–563.

Pirozzoli, S, Bernardini, M. & Orlandi, P. 2014 Turbulence statistics in couette flow at high reynolds number. *Journal of Fluid Mechanics* **758**, 327–343.

Rosteck, A. 2014 Scaling laws in turbulence - a theoretical approach using lie-point symmetries. *Doctoral thesis* .

Spalart, P. R. 1991 Spectral methods for the navier-stokes equations with one infinite and two periodic directions. *Journal of Computational Physics* **96** (2), 297–324.

Tsukahara, T., Kawamura, H. & Shingai, K. 2006 DNS of turbulent couette flow with emphasis on the large-scale structure in the core region. *Journal of Turbulence* **7**, 1–16.